NASA Technical Memorandum 85946

Aerodynamic Characteristics of the 40- by 80/80- by 120-Foot Wind Tunnel at NASA Ames Research Center

Victor R. Corsiglia, Lawrence E. Olson, and Michael D. Falarski

April 1984

National Aeronautics and Space Administration

NASA Technical Memorandum 85946

Aerodynamic Characteristics of the 40- by 80/80- by 120-Foot Wind Tunnel at NASA Ames Research Center

Victor R. Corsiglia,
Lawrence E. Olson,
Michael D. Falarski, Ames Research Center, Moffett Field, California

National Aeronautics and
Space Administration

Ames Research Center
Moffett Field, California 94035

AERODYNAMIC CHARACTERISTICS OF THE 40- BY 80-/80- BY 120-FOOT WIND TUNNEL AT NASA AMES RESEARCH CENTER

Victor R. Corsiglia,* Lawrence E. Olson,† and Michael D. Falarski‡
NASA Ames Research Center, Moffett Field, California

Abstract

A design and testing program has been undertaken to improve the aerodynamic performance of the 40- by 80-/80- by 120-Foot Wind Tunnel at NASA Ames Research Center. Experimental and theoretical results pertaining to both turning-vane performance and air-exchanger performance are presented. Extensive studies have been conducted to develop turning-vane airfoils with improved aerodynamic performance and to insure that this performance is not compromised by interactions between the cascades of airfoils and the duct or diffuser walls within which these cascades are required to operate. Much of the theoretical analysis and design was done by personnel at NASA Lewis Research Center. Because of the nature of the 40- by 80-/80- by 120-Foot Wind Tunnel complex, it was necessary to consider a wide range of vane-set designs. A design has been developed that provides efficient control of the flow at the intersection of the 40 × 80 wind-tunnel circuit and the 80 × 120 wind-tunnel circuit. The airfoil shape and solidity of this design results in a vane set that can accept onset flow at angles ranging from -5° to 55° while maintaining relatively low drag and having only minor variations in the direction of the flow exiting the cascade. A second vane set has been tested for use in a 90° bend. This cascade provides efficient aerodynamic performance yet the airfoil shape can be built using simple fabrication techniques. In a third study, it was shown that the outflow angle from a vane set is an important parameter in determining the tunnel performance downstream of the vane set. Over-turning or under-turning of the flow (measured relative to the axis of the duct or diffuser downstream from the cascade) results in cross-stream total-pressure gradients that will persist as the flow continues around the circuit of the wind tunnel. Guidelines for minimizing this potential problem are presented. An air-exchange inlet has also been designed and tested that is capable of enhancing flow quality within the wind-tunnel circuit. This air exchanger utilizes the static pressure difference between the wind-tunnel duct and the atmosphere to create a thick wall jet. One important benefit of this wall jet is improved uniformity of the flow entering the fan drive.

This paper was presented at the AIAA 13th Aerodynamic Testing Conference, San Diego, CA, March 5-7, 1984

*Assistant Branch Chief, Low Speed Aircraft Research Branch. Member AIAA.
†Aerospace Engineer. Low Speed Aircraft Research Branch. Member AIAA.
‡Assistant Branch Chief, Low Speed Wind Tunnel Investigations Branch. Member AIAA.

Nomenclature

C = vane chord

C_f = flap chord (vane set 6)

C/g = solidity, (vane chord)/gap, Fig. 8

C_p = vane surface-pressure coefficient, $(P - P_1)/(1/2)\rho U_1^2$

p = static pressure

p_T = stagnation pressure

q = dynamic pressure upstream of vane set, $(1/2)\rho U_1^2$

r = radius of curvature

Re = Reynolds number, $\rho U_1 C/\mu$

$\bar{S}$ = Stratford separation parameter

t/C = (vane thickness)/chord

U = speed of flow

W = width of duct, diffuser, or test section

x/C = coordinate parallel to vane chord

z/W = cross-stream coordinate, Fig. 2

β = vane set outflow angle, Fig. 12

$\bar{\beta}$ = average value of $\beta = \int_{-1/2}^{1/2} \beta \, d(z/w)$

δ_f = flap deflection, vane set 6, Fig. 20

ΔP_T = stagnation pressure difference across vane set, $P_{T_2} - P_{T_1}$

η = $\Delta P_T/q$, nondimensional loss coefficient

$\bar{\eta}$ = average value of $\eta = \int_{-1/2}^{1/2} \eta \, d(z/w)$

θ = angle of onset flow, Fig. 9

μ = viscosity

ρ = density of air

Subscripts

1 = conditions upstream of vane set

2 = conditions downstream of vane set

Introduction

NASA Ames Research Center has a development effort under way to expand the capabilities of the 40- by 80-Foot Wind Tunnel. Various aspects

of this activity have been reported in several earlier papers[1-8] and most recently in Ref. 9. As part of this modification, a new drive system has been installed which increases the maximum tunnel speed from 200 to 300 knots. Also, a nonreturn leg has been added to the tunnel circuit which provides a new 80 × 120 ft test section. This test section, which shares the drive system used in the 40 × 80 ft test section, will have a maximum speed of 100 knots. (These tunnels will be referred to subsequently as the 40 × 80 tunnel and 80 × 120 tunnel).

Recently, extensive additional testing and analysis have been done in an effort to refine aerodynamic load predictions in various areas of the wind-tunnel circuit and to improve aerodynamic efficiency and flow quality. This effort, which is the subject of the present paper, has resulted in new designs for several vane sets and an air-exchange system. The present paper is an overview of several ongoing projects being conducted by other investigators. Detailed descriptions of the results of these studies are being published separately.

The 40- by 80-Foot Wind Tunnel first became operational in 1944 and has been in continuous operation until the recent expansion activity. Over the years, this tunnel has been used in many aircraft development programs of national interest. These include the lifting-body reentry vehicles, such as the Space Shuttle; transport aircraft; combat aircraft; helicopters; and powered-lift vehicles of various types. After 40 yr, however, the national needs for a large-scale test facility have grown. Full-scale helicopters need to be tested at higher speeds, and powered-lift airplanes have grown larger. These factors, combined with the scheduling efficiency of a two-test-section wind tunnel led to the decision to undertake the recent major modification of the 40 × 80 Foot Wind Tunnel.

The wind tunnel is shown in plan view on Fig. 1. Vane-sets 3 and 4 are two-position (open or closed) louvers which allow air to flow in either the 40 × 80 or 80 × 120 circuit. When in the 80 × 120 configuration, vane-set 7, which is another set of two-position louvers, is open to allow the nonreturn air to exit the wind-tunnel duct. These louvers are closed in the 40 × 80 mode. Vane-sets 1, 2, 5, and 6 have been the subject of extensive additional aerodynamic studies since the publication of Ref. 9. The indraft inlet of the 80- by 120-Foot Wind Tunnel is also undergoing additional analysis and testing. The first experimental phase of the wind-tunnel tests of the inlet guide vanes (which also function as acoustic baffles) is reported in Ref. 10.

Facility, Models, and Instrumentation

1/10-Scale Vane-Set Test Facility

The channel test facility (Figs. 2 and 3) has been used extensively for two-dimensional testing of the various vane sets. Channel dimensions from the inlet through the test section are 91 cm square. Honeycomb (length = 25 cm) is installed at the inlet to suppress turbulence. Air is drawn through the channel (dynamic pressure = 22 lb/in.^{2}) by a multiblade, fixed-pitch fan (diam = 122 cm) driven by an electric motor. Reynolds number based on vane chord, Re, for a typical test was 500,000. The particular vane set under study is installed on the diagonal of the bend in the channel as shown in Fig. 2. Interchangeable channel bends allow the turning angles to be set at -5°, 45°, 50°, 55°, 60°, 90°, or 95° depending on the requirement of the particular vane set being studied. For specific applications, a 3° diffuser downstream of the vane-set location was simulated, using tapered wall inserts.

A typical set of vanes mounted in plexiglass and plates ready for installation as a unit in the channel is shown in Fig. 4. Each vane set has from 7 to 15 vanes although the most of the sets had from 8 to 10 vanes. The plexiglass-end-plates/vane combination was designed so that the angle of attack of the individual vanes could be independently set to the desired values. The vanes themselves were made of aluminum, wood, or a combination of wood and aluminum. Typically, three vanes of each cascade were pressure-instrumented with 28 to 40 static-pressure orifices per vane. These pressure-instrumented vanes were generally placed in the center region of the cascade, although the instrumentated vanes were also mounted next to the inside or outside corner of the duct to aid in studies of the interaction between the vanes and the walls of the wind tunnel. The chord length of the various vanes ranges from 6 in. to nearly 17 in. or about 1/10 the scale of the full-scale turning vanes; thus, the name 1/10-Scale Vane-Set Test Facility.

Quantitative measurements of the flow fields in the near-wakes of the cascades were obtained using a survey probe traversing the wake along a line parallel to the trailing edge of the vanes and located about 1/2 chord downstream. Both stagnation pressure and outflow angle were measured using a directional pitot-static probe. The survey probe was scanned automatically, and data were processed on-line under the control of an HP 9836 microcomputer system (Fig. 2). Other instrumentation consisted of a stationary pitot-static tube upstream of the vane set and static-pressure taps on the walls of the channel. These pressures were measured using Scanivalves and recorded using the microcomputer.

Visualization of flow separations and transition was accomplished by using oil painted on the surface of the vane or walls. This flow visualization and wake surveys obtained at several spanwise locations along the vane sets confirmed the two-dimensionality of the flow through the cascades.

A typical wake survey showing the distribution of outflow angle β and stagnation-pressure loss coefficient, $\eta = \Delta P_T/q$, is presented in Fig. 5. The wake of each of the vanes is easily discernible. The wake pressure loss rises to a maximum behind each vane and falls to a minimum downstream of the channel between vanes. The outflow angle also varies across the region between vanes. In the remainder of this paper the flow in the near-wake of a vane set will often be characterized using a spatially averaged loss coefficient, $\bar{\eta}$, and a spatially averaged outflow angle, $\bar{\beta}$.

The 1/10-scale simulation must be nearly periodic if it is to be representative of the flow

in the central region of a 30-to-40-vane cascade such as those in the actual wind-tunnel facility. It was discovered that in general the flow is not exactly periodic in the channel. However, when the angle through which the vane-set turns the flow matches the turning angle of the duct to within about 3°, there was adequate periodicity. That is, properly designed vane sets satisfy this criterion. An alternative method for obtaining $\bar{\eta}$ is to measure the streamwise drop in static pressure across the vane set. End-wall and side-wall viscous effects introduce sizeable errors in cascade loss coefficients determined by this method.

The 1/10th-scale cascade test facility has been the primary source of experimental data required for editing prospective vane-set configurations and for determining the aerodynamic loads on the vane set selected for installation in the full-scale wind tunnel.

1/50 Scale Facility

In addition to the tests conducted in the 1/10-scale channel facility, tests were also conducted in a 1/50-scale model of the full-scale facility; the model can be configured in either the 40 × 80 or 80 × 120 mode (Figs. 6a-6c). Power is provided by six multiblade, constant-pitch, axial flow fans driven by synchronous electric motors with a variable frequency supply. In the 40 × 80 mode, a speed of 127 knots can be attained in the test section; in the 80 × 120 mode, the maximum test-section speed is 55 knots.

Instrumentation consists of a survey probe for total pressure and temperature in which lateral scans are conducted at midtunnel height and at various locations throughout the wind-tunnel circuit. The total-head probe was fitted with a pressure transducer in order to provide a signal for a pen recorder. Static pressures on the walls were measured using manometer boards. Flow visualization was conducted by use of tufts on the walls of the wind-tunnel duct, on grid wires across the duct, and on a hand-held wand that could be positioned at various locations of interest. In some cases, flow-angle measurements were made with a protractor to determine the angle of a tuft mounted on a wand.

An initial concern with the 1/50-scale facility was the low Reynolds number (80,000 based on vane chord, vane-set 5, 80 × 120) which might lead to unreliable simulation of the full-scale device. It was found, however, that the small-scale facility provided very useful results qualitatively and in most cases quantitatively. For example, flow-angle measurements in the 1/50-scale model in the 80 × 120 circuit between vane-sets 4 and 5 (Fig. 1) agreed very well with full-scale data. Also, visualization of the flow near the air-exchange inlet agreed very well with full scale. The total pressure loss coefficient across the vane sets is, however, higher in the 1/50-scale than in the full-scale, but trends in the 1/50-scale agreed with computations.

Results and Discussion

Vane-Set 5 Design

A study was undertaken to provide an improved design for the vane set which is located near the intersection of the 80- by 120-Foot Wind Tunnel and the original circuit of the 40- by 80-Foot Wind Tunnel. This vane set, designated vane-set 5, is just upstream of the fan drive (Fig. 1). In the 80 × 120 mode, air flow is directed into vane-set 5 by opening vane-set 4 and closing vane-set 3. The air flow makes a 45° turn to the right at vane-set 5 in order to enter the fan drive. In the 40 × 80 mode of operation, vane-set 3 is open and vane-set 4 is closed. The flow then passes through vane-set 5 without turning. Vane-set 5 must operate in two separate modes so that it must accept inflow from two directions that differ by 45°.

Some of the vane-set configurations that were considered are shown in Fig. 7. Each configuration is sketched in both the 40 × 80 and 80 × 120 modes of operation. The designs are divided into two categories: (1) variable-geometry vane sets and (2) fixed-geometry vane sets. The remainder of this section is a brief description of studies of the variable-geometry cascades and a more detailed discussion of the development of a fixed-geometry vane set.

The aerodynamic performance of a relatively wide range of thin-plate variable-geometry configuration is reported in Ref. 8. This data base has been expanded as a result of additional testing in the 1/10-Scale Cascade Facility. The combined data base provides a means for evaluating aerodynamic performance for a range of airfoil shapes and solidities. For example, a smoothly contoured, thin airfoil with a solidity of 2.7 results in a low loss-coefficient of 0.05 in the 80 × 120 mode of operation. Other shapes such as a simple leading-edge hinged flap may result in loss coefficients as high as 0.30 for the 80 × 120 mode of operation. The anticipated range of loss coefficients for both the 40 × 80 and 80 × 120 modes of operation are shown in Fig. 7. For these types of configurations, high performance (say $\bar{\eta} < 0.15$) can be obtained only at the expense of mechanical complexity.

The tandem cascade design (Fig. 7) was estimated to have a low viscous loss-coefficient in both modes of operation ($\bar{\eta} = 0.05$). However, this design would be expensive to build because of its size and the large number of vanes required. The tandem design was, therefore, not tested in the 1/10-scale facility.

An extensive theoretical design study at Lewis Research Center that was accompanied by thorough 1/10-scale testing at Ames Research Center was carried out to develop a contoured airfoil cascade for vane-set 5 that was efficient in both the 40 × 80 and 80 × 120 modes of operation. The design process was to first use the theoretical analysis to develop several designs. From those designs the most promising configurations were selected for testing in the 1/10-Scale Cascade Facility. The analytical effort at Lewis Research Center used theoretical methods that had been developed for cascade design. These methods combine inverse inviscid-flow analysis procedures and boundary-layer theory to determine the airfoil

shape. This technique, which is described in detail in Ref. 11, has been used to develop cascade airfoils for the design conditions of vane-set 5. Panel codes, boundary-layer analysis, and empirical charts have been used to estimate off-design performance.[12]

A fixed-geometry cascade (Fig. 7) is very attractive from a structural and operation viewpoint, and two fixed-geometry airfoil cascades were designed and tested. One of these designs had a solidity of C/g of 1.6 and an airfoil with a t/C of 0.22 (design No. 1). A variable-geometry version of this airfoil is achieved by use of a two-position nose (Fig. 8a). In the 40 × 80 mode of operation the nose is up. For operation in the 80 × 120 mode, the nose of the airfoil is drooped 20°, with the hinge point located on the lower surface at a distance of 0.4 C from the leading edge of the airfoil. Measured loss coefficients for this configuration are 0.03 and 0.09 for the 40 × 80 and 80 × 120 modes of operation, respectively. The second configuration has a high solidity, $C/g = 1.9$, and a lower thickness-to-chord ratio of 0.19, (design No. 2). A direct comparison of the airfoil shapes presented in Fig. 8b shows that design No. 2 also is somewhat blunter and has additional camber in the nose region. As shown in Fig. 9, the performance characteristics for both designs is good for onset-flow angles θ ranging from -5° to 45°. For onset-flow angles greater than 45°, the performance of design No. 2 is significantly better than that of design No. 1. Some insight into the reasons for these differences can be obtained from the oil-flow visualization sketches shown in Fig. 10 and the predicted and measured surface-pressure distributions presented in Figs. 11a and 11b, respectively. For design No. 1, a relatively rapid growth of the separation bubble with increasing onset flow angle is observed. This rapid growth is probably caused by the strong suction peak in the upper surface-pressure distribution of the airfoil. Because of its higher solidity, increased nose camber, and larger nose radius, design No. 2 has a much lower suction peak (Fig. 11) and, therefore, a lower rate of growth of the separation bubble with increasing angle of onset flow.

Since vane-set 5 is located directly upstream from the fan drive of the wind tunnel, it is required that the flow-exiting vane-set 5 have an outflow angle that is within ±3°, that is, $|\bar{\beta}| \leq 3°$. This insures that the flow will be nearly aligned with the axis of the fan drives. As shown in Fig. 12, both designs satisfy this criterion for all onset angles tested.

The vane-set design that was selected for installation in the wind tunnel is the fixed-airfoil design No. 2. Although some of the variable-geometry configurations slightly outperform design No. 2, elimination of the variable-geometry requirement far outweighs the small performance penalty. And although design No. 2 requires about 20% more vanes than design No. 1, the improved performance at the higher angles of onset flow justifies selection of design No. 2.

Installation Effects Associated with Vane-Set 5

The theoretical analysis and design methods and the experimental techniques described in the preceding sections focus on the study of infinite cascades. This focus on flow that is nearly two dimensional in the spanwise direction and nearly periodic in the cross-stream direction is justified over a major region of a typical wind-tunnel vane set. Regions that violate these assumptions are in the vicinity of the vanes located nearest to the side walls of the wind tunnel. The strong interaction between the walls and the vanes in that region will affect the performance of the vane itself and, more importantly, affect the viscous flow on the walls of the wind tunnel. These interactions, which are called installation effects, occur at both ends of the vane sets. For the concave corner, the regions of separated flow, if they exist at all, are generally confined to the immediate vicinity of the cascade. This is not necessarily true for the flow around the convex corner where catastrophic separation of the boundary layer on the wall can extend well downstream from the cascade. Because of the distance from the 45° concave corner at vane-set 5 to the inlet of the fan drive is less than one-third of the width of the diffuser, it is essential that the flow around the corner be controlled so that significant distortion of the flow into the fans does not occur. After considering several techniques for achieving this objective, the use of a wall fairing extending down from the corner was selected. The remainder of this section briefly describes the theoretical design method used to develop the fairing shape and presents experimental results obtained to confirm that the resulting aerodynamic performance is acceptable.

The analysis of the flow in the vicinity of the corner (Fig. 13) uses a panel code for two-dimensional flow to compute the pressure distribution on the wall of the wind tunnel. Knowing this pressure distribution and the boundary-layer characteristics upstream from the corner, Stratford's method,[13] is then used to test for flow separation that may occur in the vicinity of the cascade or downstream between the cascade and the inlet to the fan face.

The design procedure has control over three geometric characteristics:

1) The shape of the fairing (the length of the fairing was specified by the proximity of vane-set 5 to the inlet to the fan drive)

2) The position of the cascade (it could be moved as a unit relative to the 45° corner)

3) The angle of attack of the individual vanes

The design procedure is to minimize the Stratford flow-separation criterion $\bar{S}$ as follows:

1) Suppose a cascade position and vane angles of attack; then iterate the fairing shape to minimize $\bar{S}$

2) Hold the fairing shape and the vane angles of attack constant, and iterate the cascade position (two parameters) to minimize $\bar{S}$.

3) Hold the fairing shape and cascade position constant, and iterate the angle of attack of the vanes to minimize $\bar{S}$; the aerodynamic performance of the vanes constrains this motion

4) Repeat steps (1) - (3) as necessary.

The optimum geometry that was determined using this analytical procedure is denoted in Fig. 13. Also shown in this figure are several "nonoptimum" fairing shapes. As one might expect, the pressure distributions on the wall are sensitive to fairing shape and to the angle of attack of the vanes. The pressure distribution was not quite as sensitive to cascade position. It should be noted that although the design procedure emphasizes performance in the 80 × 120 mode of operation, the optimized configuration must also perform well in the 40 × 80 mode.

Verification tests of this design have been conducted in the 1/10-Scale Cascade Facility. These tests focus on the wall boundary layer and the wakes of the vanes nearest the inside wall. This installation is shown in Fig. 14a for the 80 × 120 mode and in Fig. 14b for the 40 × 80 mode. Flow surveys were made at the upstream and downstream locations noted in the figure. Results of surveys appear on Figs. 15a and 15b for the 80 × 120 and 40 × 80 modes, respectively. For these tests, the flow was also visualized with tufts and with oil, and it was confirmed that boundary-layer separation did not occur. Also, for these tests the upstream boundary layer was artificially increased from that which would otherwise have occurred in the test facility. This was done to simulate the boundary layer that was estimated to be present in the actual tunnel installation. The boundary-layer thickening was accomplished by installing tailored screens upstream of the flow-straightening honeycomb shown in Fig. 2. These screens extended from the inner wall of the channel into the flow sufficiently far to generate the desired boundary-layer profile just upstream of vane-set 5 at the boundary-layer survey location noted in Fig. 14. Figures 15a and 15b show that the boundary-layer loss coefficient downstream of the vane set was still large compared with the loss in the wake of one vane. However, the fairing has kept the increase in wall loss-coefficient across the vane set to a minimum. The presence of the fairing greatly reduced the loss relative to the case without the fairing (not shown) in the 80 × 120 mode, and also reduced the wall loss slightly in the 40 × 80 mode.

Surveys were also made of the total pressure losses near the wall downstream of vane-set 5 on the other side of the wind tunnel from that just discussed where the flow turns an inside corner. The flow disturbances in this region were found to be minimal, and a fairing was unnecessary. However, tests were made to determine the optimum gap between the wall and the outermost vane, with the objective of minimizing losses associated with this concave corner.

Van-Sets 1, 2, and 8 Design

As a result of an increase in wind-tunnel test-section speed from 200 to 300 knots, the aerodynamic loads on the fixed-geometry vane-sets 1, 2, and 8 (Fig. 1) were increased by a factor of about 2.25. It was determined from a structural analysis that vane-set 8 did not need to be upgraded in the modification because it could adequately support the increased loads. Vane-sets 1 and 2, however, had inadequate structural strength margin and needed to be replaced. Tests were, therefore, conducted on the existing design vane set to determine whether any change in the aerodynamic design was warranted.

In the original wind tunnel, vane-sets 1, 2, and 8 had the same airfoil shape and solidity. The only difference between them was that the vane-set 1 and 2 airfoils had chords of 1.83 m (6 ft), whereas the vane-set 8 airfoils have chords of 0.91 m (3 ft). The shape of all airfoils consisted of circular arcs for the upper and lower surfaces and a circular-arc nose. Testing of this cascade design in the 1/10-Scale Cascade Facility gave a measured loss coefficient of $\bar{\eta} = 0.092$, which is a relatively efficient design. However, two other undesirable characteristics were found. These were a slight overturning of the flow and a reversal of pressures between the upper and lower surface on the nose (Fig. 16). Lewis Research Center, therefore, undertook a theoretical study to modify the design to correct these deficiencies. Calculations of the pressure distribution of the original design agreed well with the measurements (Fig. 16). The overturning of the flow was also predicted. However, the predicted overturning was slightly greater than that measured (3.5° versus 2°). This difference is attributable to the effect of the boundary layer on the upper-surface trailing edge, which is not accounted for in the theory. The resulting revised design (Fig. 17) had about 15° of vane camber (angle between camberline at nose and camberline at tail) removed and the nose radius was increased over that of the original design (not shown). The use of circular arcs to determine aerodynamic shape was retained. The measured value of loss coefficient was $\bar{\eta} = 0.07$, which is an improvement over what had already been an efficient design. The predicted turning of the flow was 0° and the measured underturning was 2°. This maintains the same theory-measurement difference as noted above for the original design. It is expected that the increased Reynolds number of the full-scale installation from that of the 1/10-scale tests will result in an additional 1.0° of turning. This would change the 2° of underturning to 1° of underturning, which is an acceptable design. The pressure distribution on the revised design (Fig. 18) no longer reversed load on the nose, and the adverse pressure gradients near the nose was significantly reduced.

Vane-Set 6 Design

Vane-set 6 is the vane set downstream of the fan drive (Fig. 1). It can be configured in either of two orientations depending on whether the 40 × 80 or 80 × 120 circuit is being used. The design of the vane set (Fig. 19) consists of a fixed uncambered vane which is aligned with the fan drive and is acoustically treated to reduce the transmission of fan-drive noise to the community when the 80 × 120 circuit is being used. When in the 80 × 120 mode, the trailing-edge flaps are undeflected and aligned with the fixed portion of the vane set. The air flow is then directed through vane-set 7, which is open, and allowed to leave the tunnel duct. In the 40 × 80 mode, vane-set 7 is closed, and the flaps are deflected about 90° so that the flow is directed toward vane-set 8.

The tests in the 1/10-scale channel on vane-set 6 included flaps with three different chord lengths and various flap deflection angles. It was found that the outflow angle from the vane set was very dependent on the flap chord length that was used. For example, for the shortest of the flaps tested ($C_f/C = 0.22$, $\delta_f = 90°$), the flow was underturned by 13°. When the flap chord was doubled ($C_f/C = 0.36$, $\delta_f = 90°$), however, the flow was overturned by 12°. Setting this longer chord flap to a deflection $\delta_f = 80°$ aligned the flow approximately in the 1/10-scale facility (Fig. 20).

A similar result is shown in Fig. 12 for vane-set 5. When the onset angle was varied from 45° to 60°, the resulting outflow angle changed from an underturning to an overturning. It is to be noted that the increase in flow-turning angle is greater than the increase in duct-bend angle. This overturning characteristic was also measured on some of the thin airfoil vane-set configurations considered for use in vane-set 5. Cascades in which this phenomenon is observed always have large amounts of separated flow on the airfoils. In contrast to this, cascades with little or no separation on the airfoils are observed to exhibit the more classical behavior; that is, reduced turning angle (measured relative to the chord line of the airfoil) resulting from increased loading of the airfoil. The turning of the flow beyond what would be predicted from potential-flow analysis is probably related to the separation, turbulent mixing, and reattachment process in the flow between the airfoils.

Since it is essential that the flow be nearly uniform in the test section of the 40 × 80 wind tunnel, it is important that the flow-exiting vane-set 6 be nearly uniform. When the outflow from vane-set 6 is aligned with the outflow duct ($\bar{\beta} = 0°$), the flow is periodic, as can be seen in Fig. 21a, which shows data from the 1/10-scale channel. For this configuration, vane-set 6 would not be expected to be a source of flow nonuniformity in the test section. Figure 21b shows similar data for a configuration with 13° of underturning. In this case the stagnation-pressure distribution is no longer periodic, and there is a significant net gradient in total pressure loss across the channel. Similarly, overturning the flow produces a gradient of opposite sign, with the largest losses occurring on the outside of the turn (Fig. 21c). The gradient of the loss coefficient, $\partial\eta/\partial(z/W)$, has been estimated by fitting a straight line through the η versus z/W curves, as shown in Fig. 21b. The effect of flow-turning angle on the cross-stream gradient in stagnation pressure is summarized in Fig. 22. For the range of flap chords and flap deflections considered, there is a nearly linear relationship between gradient in loss coefficient and angle of outflow. Tests were also conducted in the 1/50-scale model to investigate further the implications of the total-head loss gradient discussed above. The measured outflow angle β is shown in comparison with the 1/10-scale data in Fig. 20 for the three configurations tested. As shown, there was 3°-4° additional turning in the 1/50-scale facility. This small difference provides confidence in the 1/50-scale results.

Further tests were conducted using the 1/50-scale facility to determine the effect of a nonuniform total-head generated by vane-set 6 on the dynamic pressure distribution across the wind-tunnel duct at various locations around the tunnel circuit. It was found that different outflow angles from vane-set 6 resulted in different lateral distributions in dynamic pressure in the test section (Fig. 23a). The larger gradient in dynamic pressure shown ($\bar{\beta} = -15°$) is excessive for a good wind-tunnel design. Downstream of the test section past the first turning vane, the lateral gradient is amplified (Fig. 22b). Excessive flow distortion at this tunnel duct location can cause poor fan-drive performance and excessive fan vibration.

Another parameter in the evaluation of the performance of vane-set 6 is the average loss coefficient, $\bar{\eta}$. Test-section maximum velocity is a relatively weak function of $\bar{\eta}$. For example, reducing $\bar{\eta}$ from 1.6 to 0.8 will result in a 2% increase in maximum test-section velocity (constant power). Of course the drag load and, therefore, the required structural strength of the vane set are directly dependent on $\bar{\eta}$. An important parameter affecting $\bar{\eta}$ is the flap chord. Figure 24 shows the effect of flap chord on loss coefficient for the case in which the flow exiting the vane set is aligned with the outflow duct. As can be seen from this figure, the loss coefficient of the vane set (with full turning) is strongly dependent on the chord of the flap. Increasing the flap-chord/vane-chord ratio from $C_f/C = 0.22$ to $C_f = 0.36$ reduces the loss to less than 40% of its original value.

Air-Exchange Inlet Design

The purpose of the 40 × 80 tunnel air-exchange system (Fig. 1) is to reduce the concentration in the wind-tunnel air of exhaust products from the engines or powered models under test in the test section and to reduce tunnel temperature. Tunnel temperature can become excessive as a result of frictional heating of the air in the wind-tunnel duct, heat from the fan-drive electric motors, and heat from the exhaust of model engines in the test section. Analysis of the energy balance in the wind-tunnel duct coupled with the past operational experience with tunnel temperature versus time in the full-scale tunnel led to the determination that the required air-exchange rate was to be up to a maximum of 10% of the flow rate in the wind-tunnel duct.

The 1/50-scale facility and a two-dimensional panel code were used to design an air-exchange inlet at the location noted in Fig. 1. The technique in the theoretical work was to use the Stratford criterion to identify configurations that did not exhibit flow separation in a manner of the vane-set 5 wall-fairing work discussed above. The objective of the design effort was to provide a uniform total-head distribution entering the fan drive and to minimize the power loss associated with the air-exchange system. It was also required that the design be such that test-section flow quality was acceptable. The design selected (Fig. 25) is a large door that spans from floor to ceiling and opens into the tunnel duct. Air enters the tunnel duct because of the static pressure difference between the inside and outside of the structure and forms a jet parallel to the duct wall. The result is a wall jet located on the inside wall (courtyard wall) of the wind tunnel. Surveys of the dynamic pressure

distribution were made at the air-exchange inlet, fan-drive inlet, and test section (Fig. 26). The enhancement of the velocity profile at the fan-inlet location is evident. It was found, as shown, that the dynamic pressure profile in the test section was insensitive to the air-exchange inlet design. This insensitivity in the test section was found to exist for a wide range of design and test conditions. The designs tested include the one shown on Fig. 25, but located on either or both sides of the tunnel. The design shown on Fig. 25 was selected because it provided the most uniform profile at the fan-drive inlet. The wind-tunnel boundary layer with the air exchanger closed at the fan-drive inlet is more distorted near the inside wall of the tunnel than near the outside wall; therefore, the air-exchange inlet jet would be expected to be most beneficial along the inside wall of the tunnel duct.

Another concern with the air-exchange design which was investigated is its effect on the temperature distribution in the test section. An excessive distortion of the test-section temperature profile would be unacceptable. Surveys of test-section temperature were made in the 1/50-scale facility. With the air exchanger closed, the temperature of the flow is usually higher than the normal room air temperature because of the frictional heating of the air and the heat from the electric-drive fan motors. A typical available temperature difference between the tunnel and the room air was 20°F. It was found (Fig. 27) that the temperature distribution across the tunnel test section was nearly uniform for various air-exchange inlet designs. It has been concluded from this study that a single wall-jet type of air-exchange inlet located as shown on Fig. 1 will provide sufficient air exchange to reduce flow distortions at the fan inlet and maintain the required quality of flow in the test section.

Concluding Remarks

A design and testing program directed at providing an improved aerodynamic design of the 40 × 80/80 × 120-Foot Wind Tunnel at NASA Ames Research Center was discussed. This program focused on the design of the vane sets that provide the turning of the flow at the corners of the wind tunnel. In addition, the aerodynamic design of an inlet of an air-exchange system and the effect of that inlet throughout the wind-tunnel circuit were described. This air-exchange system serves to control the air temperature and the concentration of pollutants in the wind tunnel. In this activity, extensive use has been made of two- and three-dimensional, inviscid, panel computer codes along with boundary-layer analysis. Also, testing was done using a 1/10-scale two-dimensional facility and a 1/50-scale three-dimensional model of the entire wind tunnel. The objective of these calculations and tests was to provide an improved aerodynamic design and an accurate determination of the aerodynamic loads on the wind-tunnel components. It was found that these theoretical and experimental tools are very reliable in producing excellent designs, and there was excellent agreement between theory, scale-model measurements, and full-scale measurements.

A new fixed-geometry vane set was developed for the 45° intersection of the 40 × 80 and 80 × 120 tunnel circuits. It has been shown that this design produces low drag and the same outflow direction at onset flow directions that vary over a range of more than 45°, depending on whether the 40 × 80 or 80 × 120 tunnel is used. The contour shape for the airfoils in this cascade was obtained by personnel from Lewis Research Center, using computer codes that were developed for use in turbomachinery cascade design.

Another study focused on the design of vane sets for 90° turns. For the vane sets that operate in only a single mode, a design was selected that features simple geometry. The contour of the airfoils of the cascade is described by circular arcs for the upper surface, lower surface, and nose. It was found that the design that was determined by theoretical analysis and then tested for a range of conditions was efficient and tolerant to off-design conditions. For another vane set, the outflow direction varied by 90°, depending on whether the 40 × 80 or 80 × 120 circuit was being used. This is a variable-geometry vane set that consists of an acoustically treated fixed vane and a movable trailing-edge flap. It was shown, using the 1/10-scale channel and the 1/50-scale three-dimensional facilities, that the outflow angle from this vane set affects the quality of the flow in the test section and other locations in the wind-tunnel circuit. An overturning or underturning of the flow by the vane set causes a nonuniform lateral distribution of dynamic pressure.

Finally, an air-exchange inlet was designed that improved the flow quality entering the fan drive. This design was found to provide smooth flow entering the wind-tunnel circuit and no loss of flow quality in the test section.

Acknowledgements

The work reported herein is a combined effort from personnel at Ames Research Center in the Low Speed Aircraft Research and Low Speed Wind Tunnel Investigation Branches and from Lewis Research Center in the Computational Fluid Mechanics and Fan-Compressor Branches. In particular, the efforts of Eric McFarland and Jose Sans is gratefully acknowledged.

References

[1]Kelly, M. W. and Hickey, D. H., "Requirements and Design Considerations for a New Full-Scale Subsonic Wind Tunnel," NATO Seminar on General Problems Relating to Aerodynamic Testing Facilities, Institute Franco Allemand de Recherches de Saint-Louis, France, May 4-7, 1971.

[2]Kelly, M. W., Mort, K. W., and Hickey, D. H., "Full-Scale Subsonic Wind Tunnel Requirements and Design Studies," NASA TM X-62, 184, 1972.

[3]Kelly, M. W., McKinney, M. O., and Luidens, R. W., "The Requirements for a New Full-Scale Subsonic Wind Tunnel," NASA TM X-62,106, 1972.

[4]Kelly, M. W., "Meeting the Challenge of Advanced Helicopters," Vertiflite Magazine, Vol. 19, Mar./Apr. 1973, pp. 4-8.

[5]Williams, J., Proceedings of AHS Panel Discussion on the Requirements for a New Large Subsonic Wind Tunnel for Research and Development Testing on V/STOL Aircraft, Oct. 1972, also RAE Technical Memorandum Aero. 1472, Jan. 1973.

[6]Mort, K. W., Kelly, M. W., and Hickey, D. H., "The Rationale and Design Features for the 40- by 80-/80- by 120-Foot Wind Tunnel," Paper 9, AGARD Conference Proceedings 174 on Wind Tunnel Design and Testing Techniques, AGARD-CP-174, Oct. 6-8, 1975.

[7]Mort, K. W., Soderman, P. T., and Eckert, W. T., "Improving Large-Scale Testing Capability by Modifying the 40- by 80-Foot Wind Tunnel," AIAA Journal of Aircraft, Vol. 16, No. 8, Aug. 1979, pp. 571-575.

[8]Eckert, W. T., Wettlaufer, B. M., and Mort, K. W., "The Aerodynamic Performance of Several Flow-Control Devices for Cluttered Flow Systems," NASA TP-1972, 1982.

[9]Mort, K. W., Engelbert, D. F., and Dusterberry, J. C., "Status and Capabilities of the National Full-Scale Facility," AIAA Paper 82-0607, Williamsburg, Va., Mar. 1982.

[10]Dudley, Michael R., Unnever, Gregory, and Regan, Dennis R., "Two-Dimensional Wake Characteristics of Inlet-Vanes for Open-Circuit Wind Tunnel," AIAA Paper 84-0604, San Diego, Calif., Mar. 1984.

[11]Sans, Jose et al., "Design and Performance of a Fixed Nonaccelerating Guide-Vane Cascade that Operates over an Inlet Flow Range of 60°, NASA TM-83519, 1983.

[12]McFarland, E., "A Rapid Blade-to-Blade Solution for Use in Turbomachinery Design," NASA TM-83010, 1983.

[13]Stratford, B. S., "The Prediction of Separation of the Turbulent Boundary Layer," Journal of Fluid Mechanics, Vol. 5, 1959, pp. 1-16.

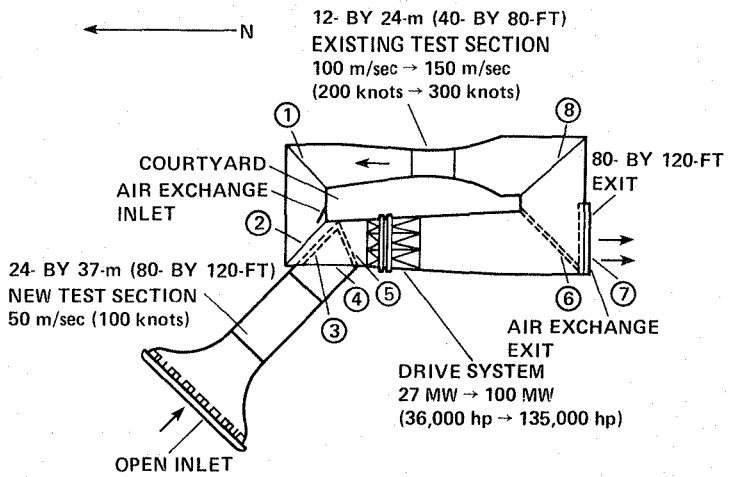

Fig. 1 Schematic of 40- by 80-/80- by 120-Foot Wind Tunnel at NASA Ames Research Center.

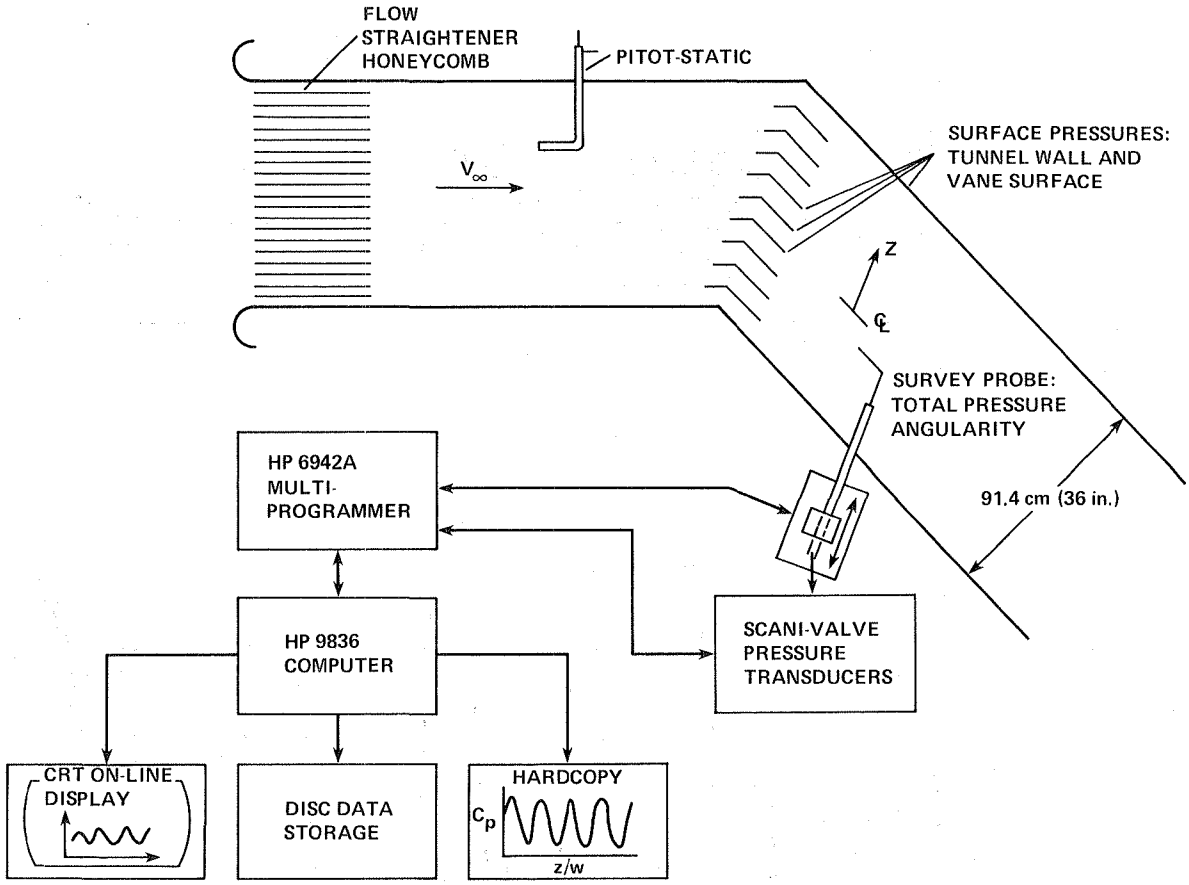

Fig. 2 Schematic of 1/10-scale channel facility and instrumentation.

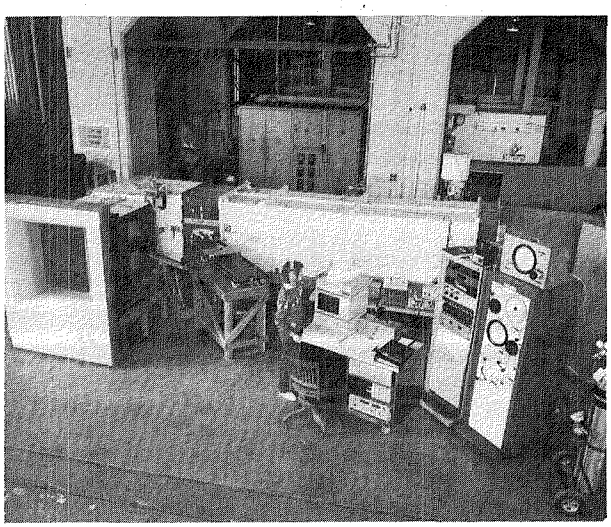

Fig. 3 The 1/10-scale channel facility.

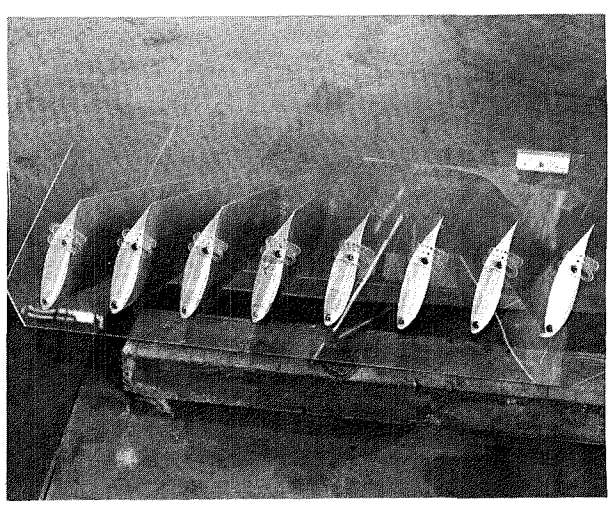

Fig. 4 Vane-set 5 design shown removed from the 1/10-scale channel facility.

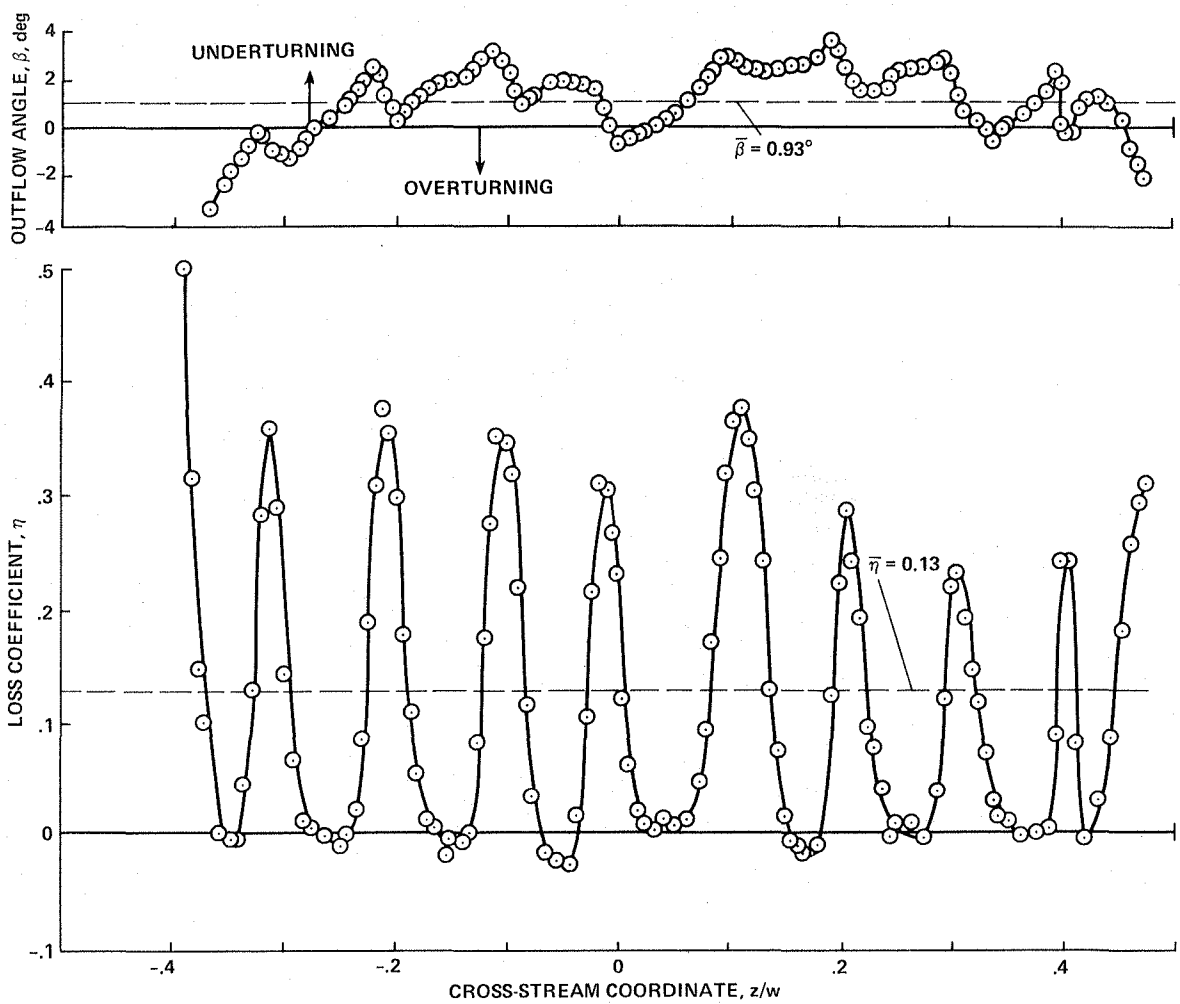

Fig. 5 Typical data on outflow angle β and loss coefficient η from the 1/10-scale channel facility.

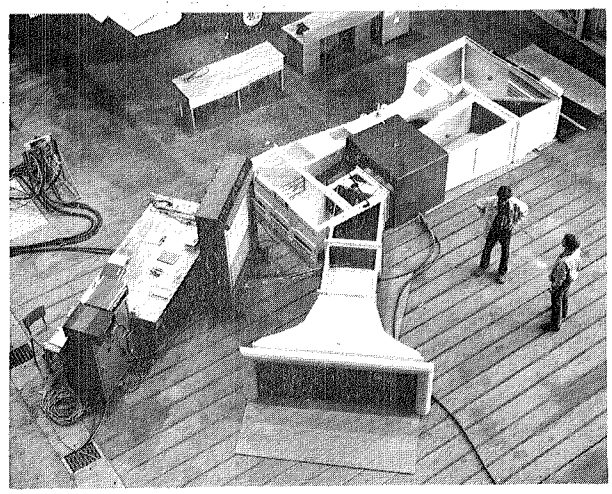

a) Top view.

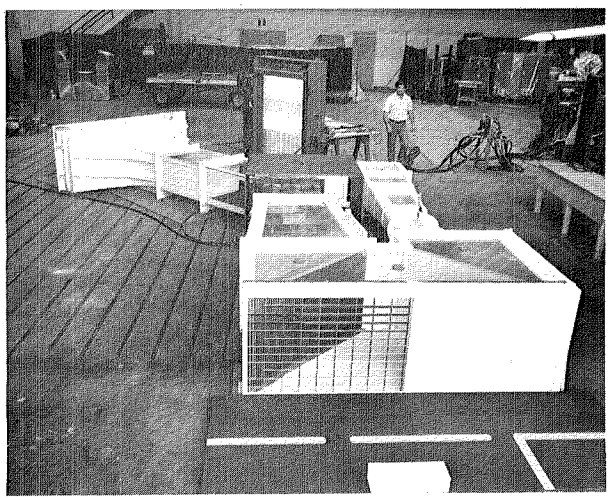

b) View of 80 × 120 exit.

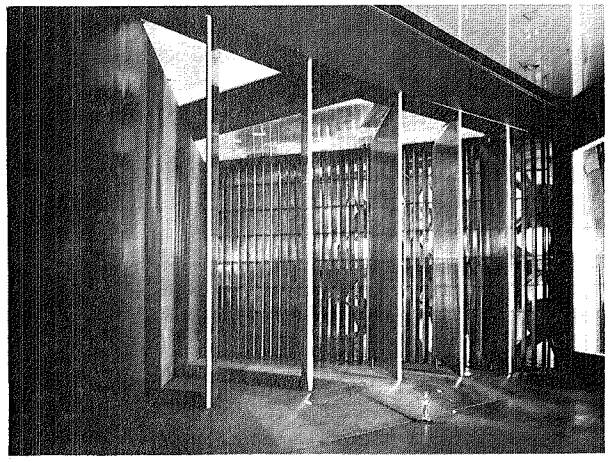

c) View from inside 80 × 120 duct looking downstream through vane-set 4 at vane-set 5 (flat plate design).

Fig. 6 The 1/50-scale three-dimensional facility.

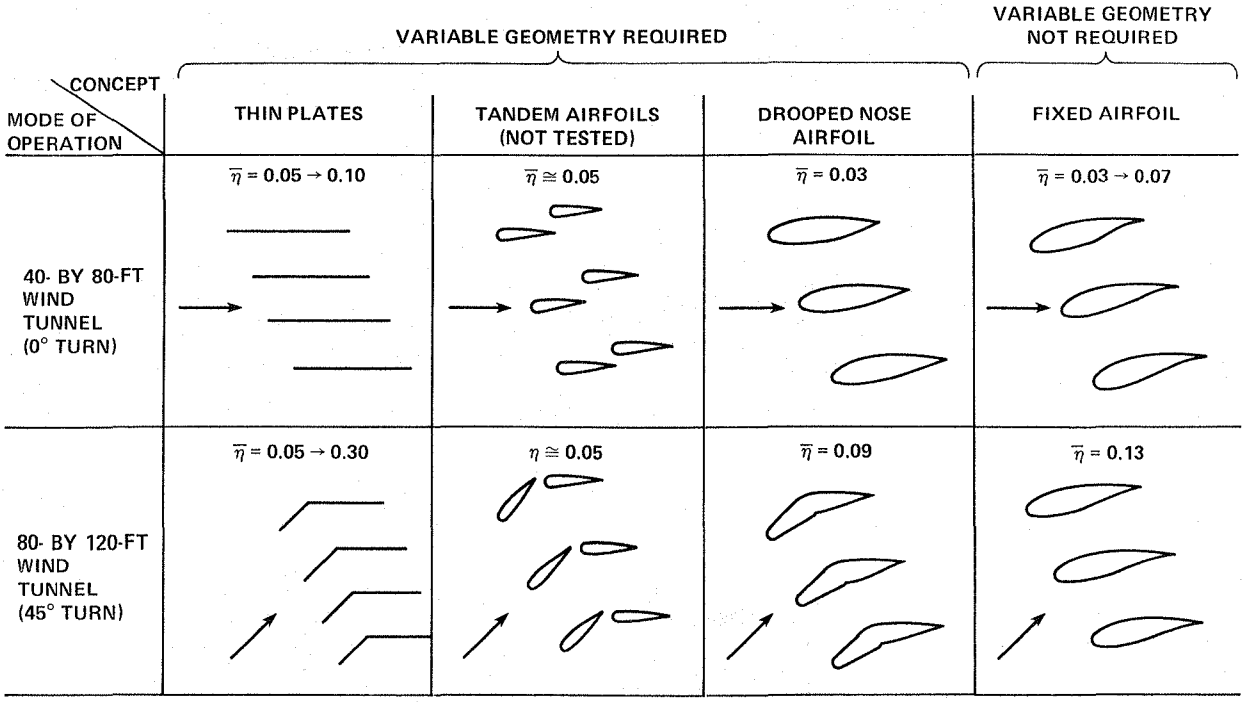

Fig. 7 Candidate configurations investigated for vane-set 5.

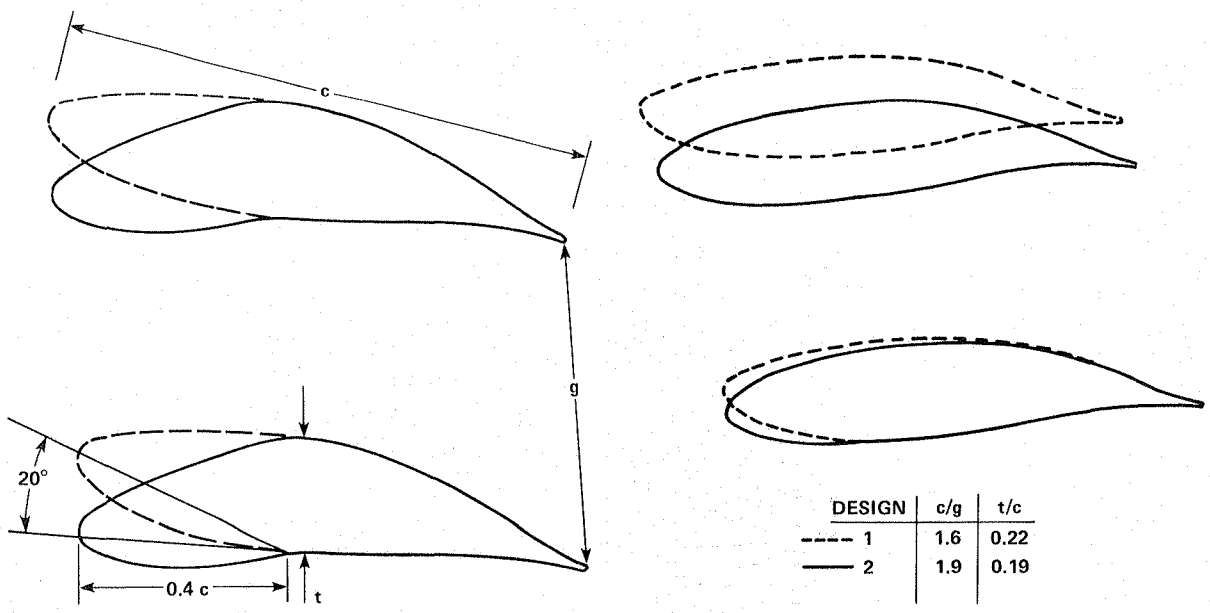

a) Drooped-nose design, σ = 1.6, t/C = 0.22.

b) Fixed-geometry designs Nos. 1 and 2.

Fig. 8 Vane-set 5 contoured vane configurations.

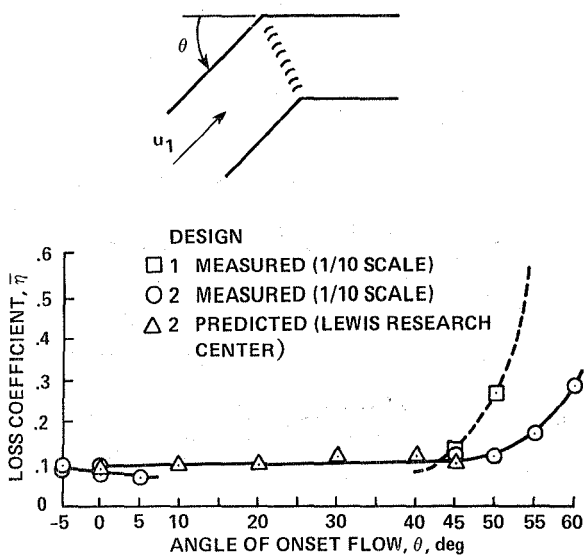

Fig. 9 Effect of onset-flow angle and vane design on loss coefficient; vane-set 5 fixed-geometry design, 1/10-scale channel facility.

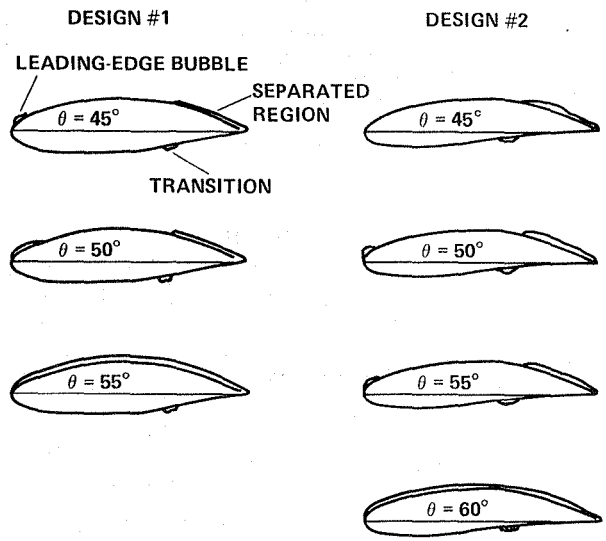

Fig. 10 Effect of design and onset-flow angle on flow separation and transition characteristics: oil-flow visualization results from 1/10-scale channel facility; vane-set 5 fixed-geometry designs Nos. 1 and 2.

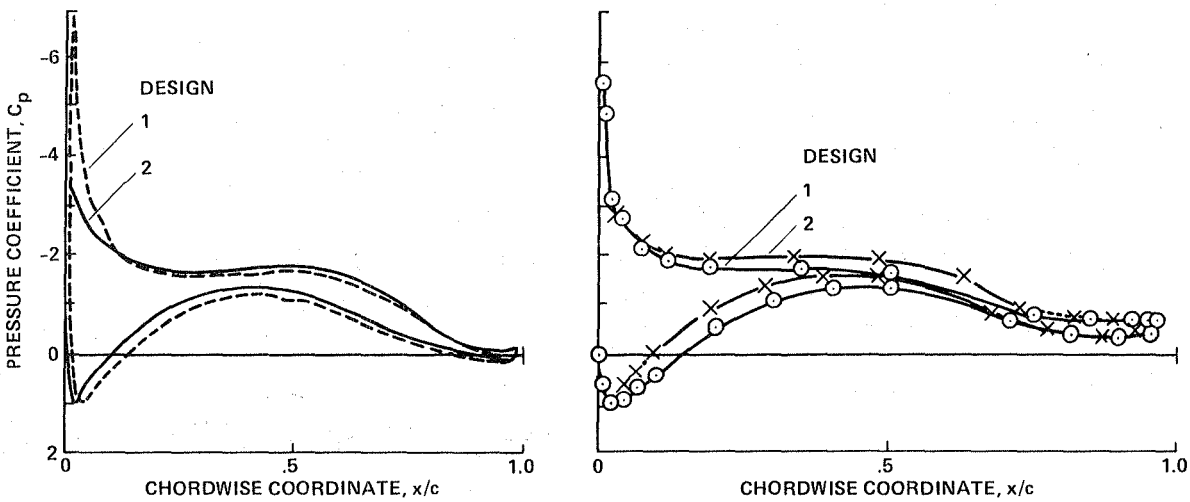

a) Predicted with inviscid panel code.

b) Measured in 1/10-scale channel facility.

Fig. 11 Chordwise pressure coefficient distribution on vane-set 5 fixed-geometry designs.

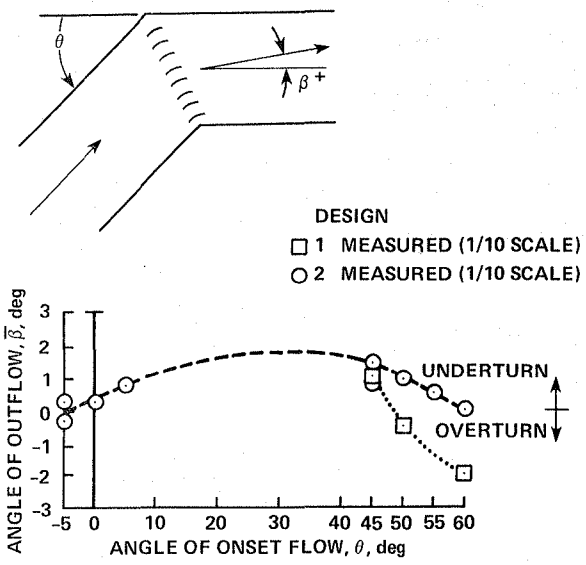

Fig. 12 Effect of onset-flow angle and design on outflow angle: vane-set 5, fixed-geometry designs Nos. 1 and 2.

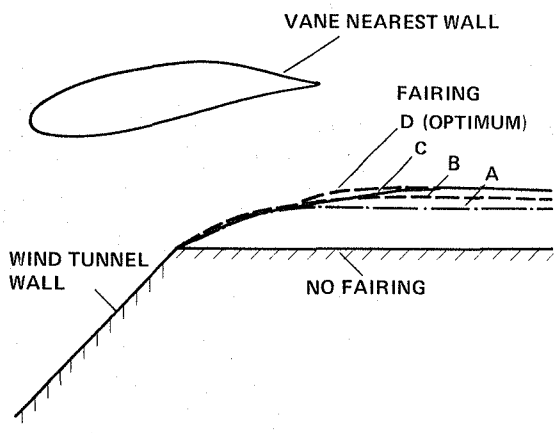

Fig. 13 Wall-fairing shapes investigated theoretically (inviscid panel code): vane-set 5 fixed-geometry design No. 2.

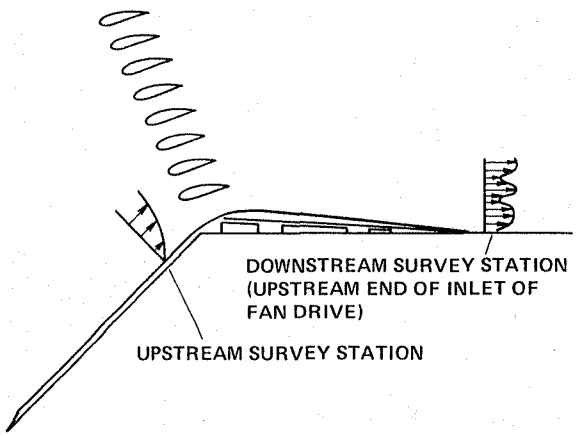

a) 80 × 120 mode.

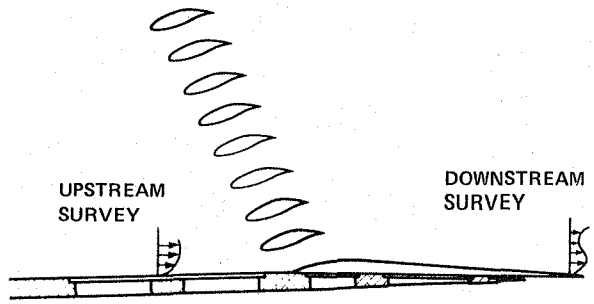

b) 40 × 80 mode.

Fig. 14 Sketch of wall-fairing installation in 1/10-scale channel facility (boundary-layer measurement locations are noted).

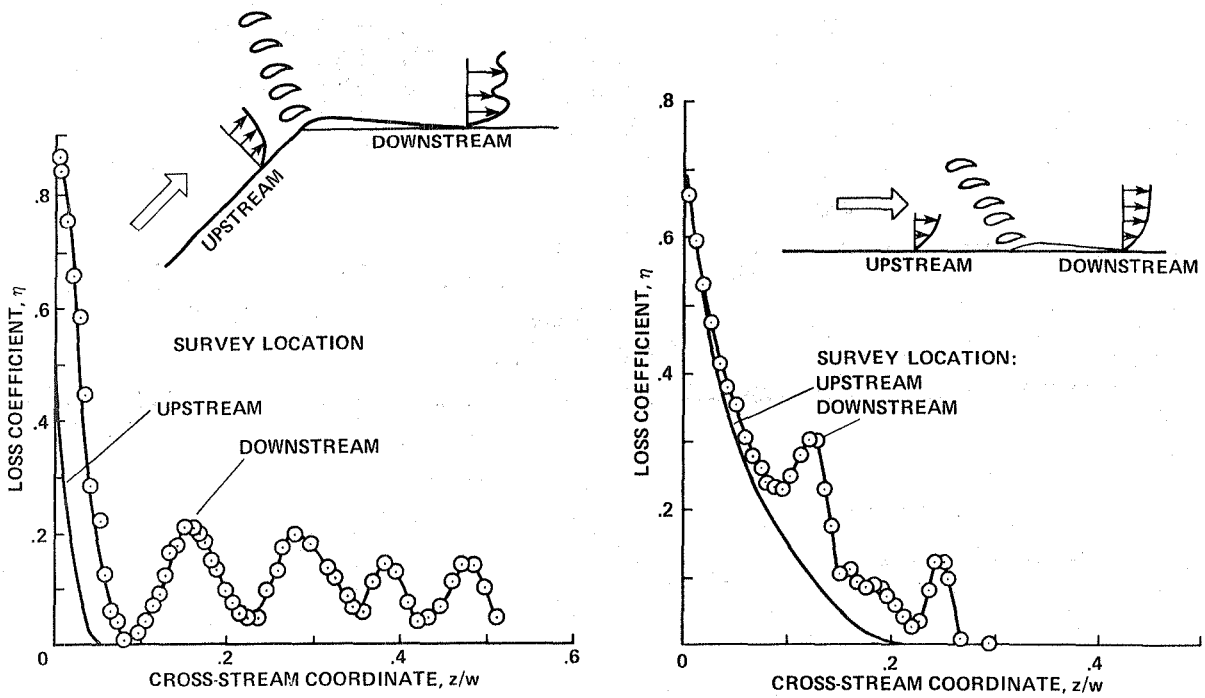

a) 80 × 120 mode.

b) 40 × 80 mode.

Fig. 15 Change of loss-coefficient profile near wall across vane-set 5; wall fairing installed, 1/10-scale channel facility.

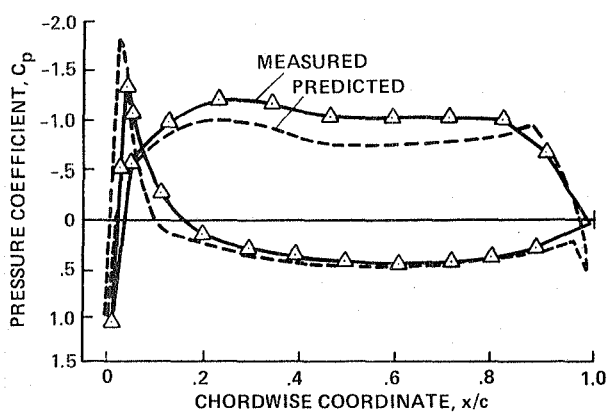

Fig. 16 Chordwise pressure coefficient distribution on the original design of vane-sets 1 and 2, predicted by inviscid panel code; measured in 1/10-scale channel facility.

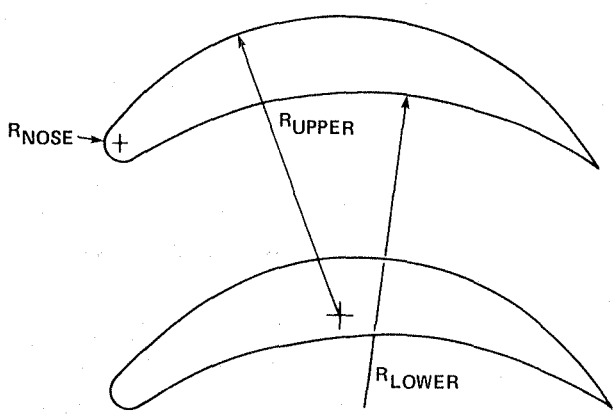

Fig. 17 New design for vane-sets 1 and 2.

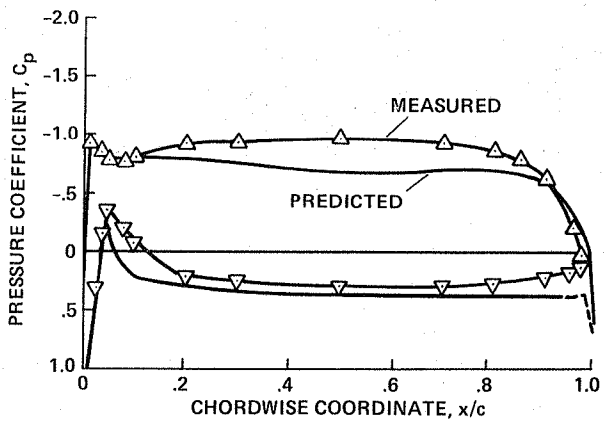

Fig. 18 Chordwise pressure coefficient distribution on new design of vane-sets 1 and 2; predicted by inviscid panel code, measured in 1/10-scale channel facility.

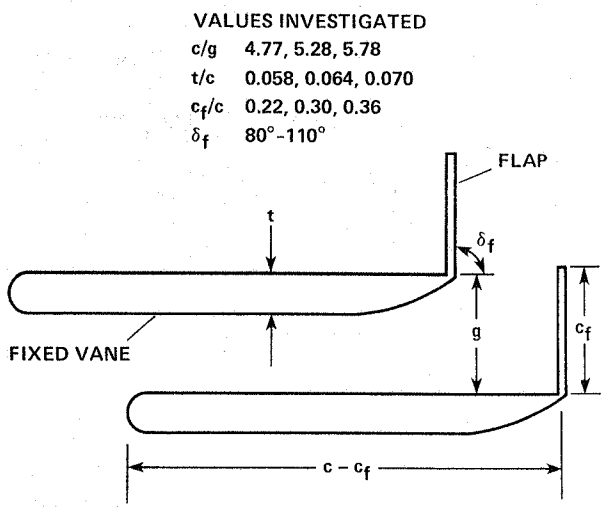

Fig. 19 Vane-set 6 design.

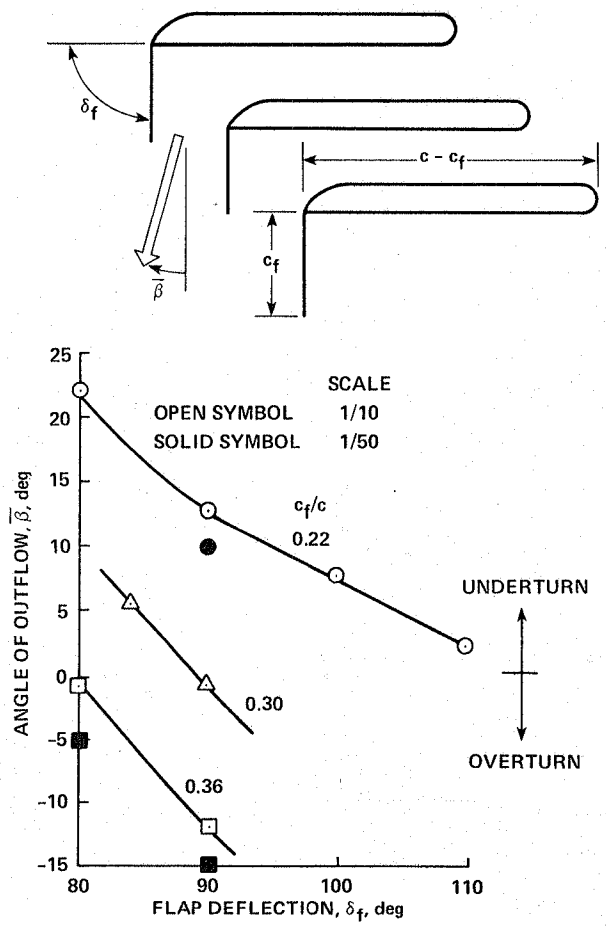

Fig. 20 Effect of flap chord and deflection on angle of outflow ($\bar{\beta}$): vane-set 6, 1/10-scale and 1/50-scale facilities, 40 × 80 mode.

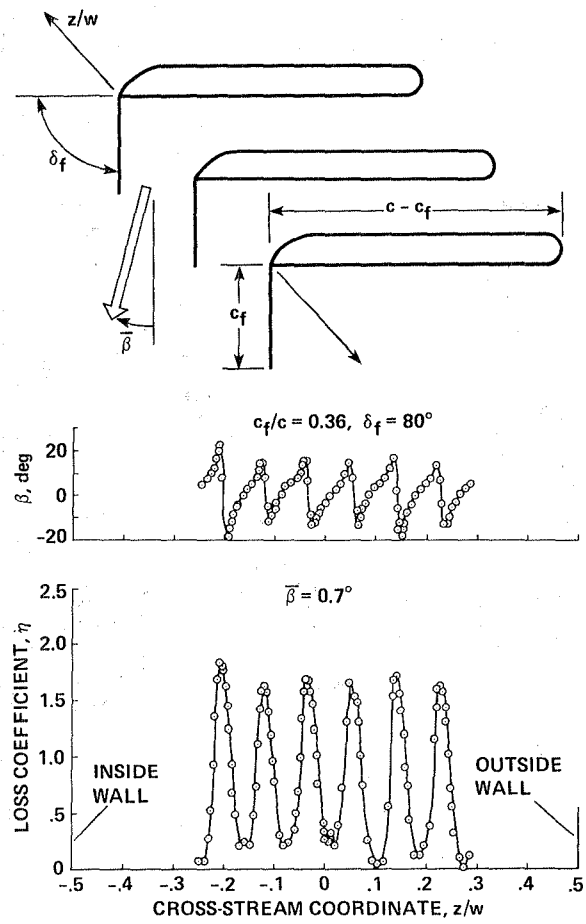

a) Outflow aligned with duct ($C_f/C = 0.36$, $\delta_f = 80°$).

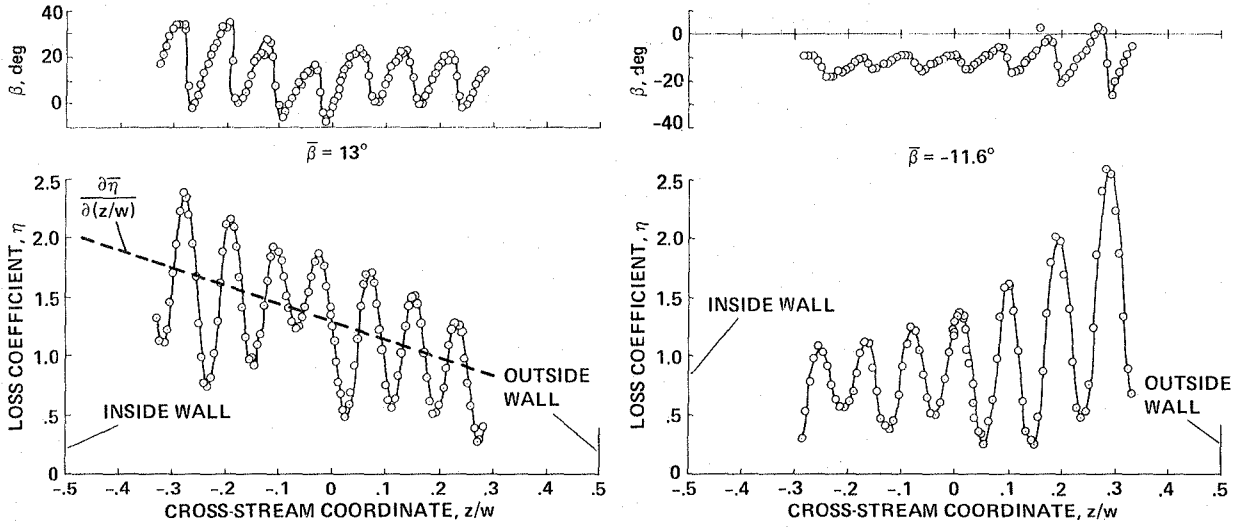

b) Underturn ($C_f/C = 0.22$, $\delta_f = 90°$).

c) Overturn ($C_f/C = 0.36$, $\delta_f = 90°$).

Fig. 21 Typical data from 1/10-scale channel facility showing relationship between outflow angle and total-pressure-loss gradient across wind-tunnel duct.

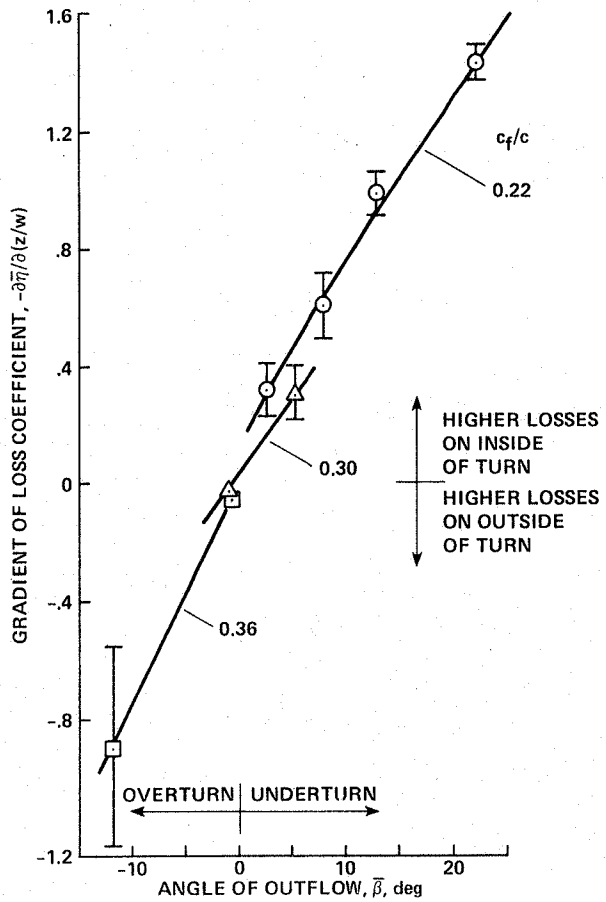

Fig. 22 Effect of flow-turning angle on the cross-stream gradient in loss coefficient: vane-set 6, 40 × 80 mode, 1/10-scale channel facility.

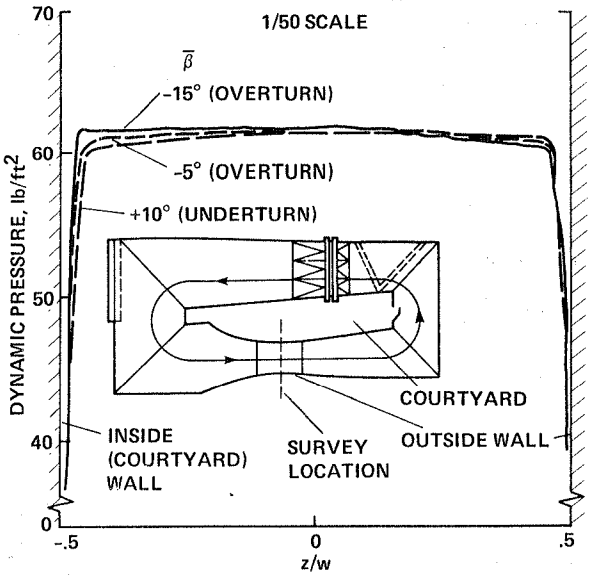

a) Flow surveys in test section of 40 × 80 tunnel.

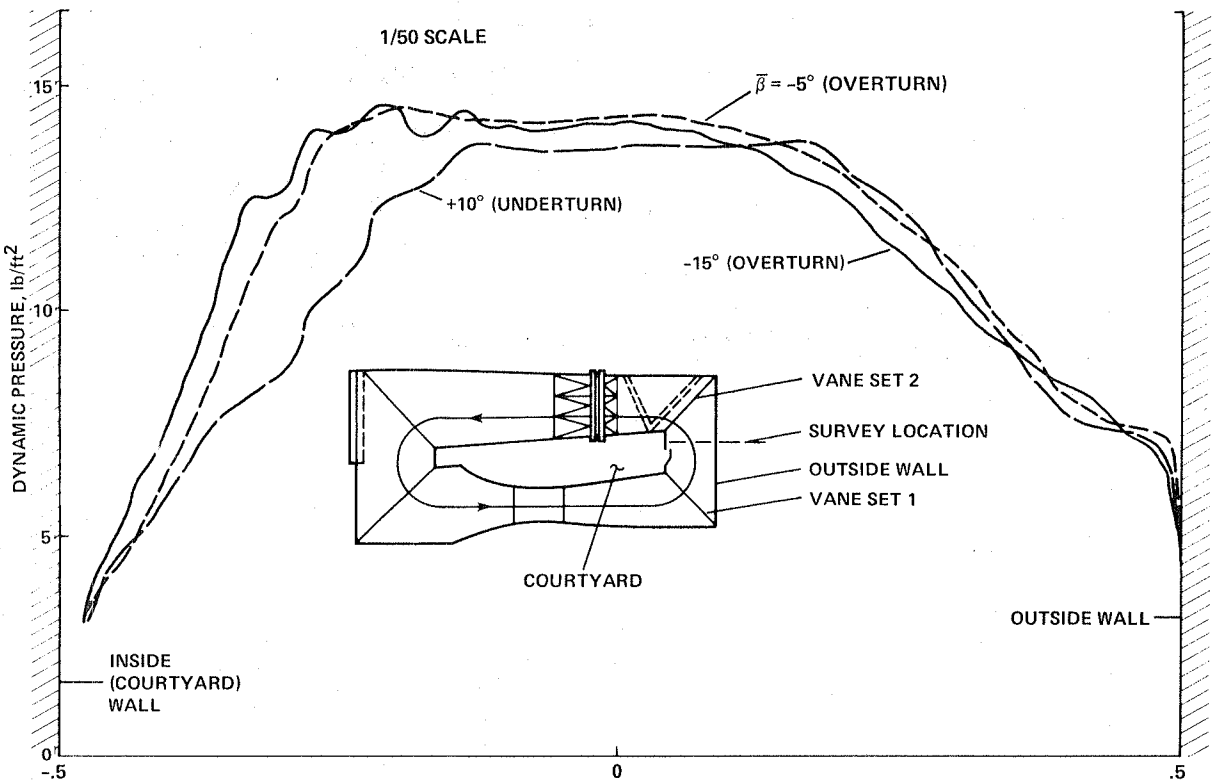

b) Flow surveys between vane-sets 1 and 2.

Fig. 23 Effect of outflow angle $\bar{\beta}$ from vane-set 6 on the total-pressure profile across the wind-tunnel duct: 1/50-scale three-dimensional facility.

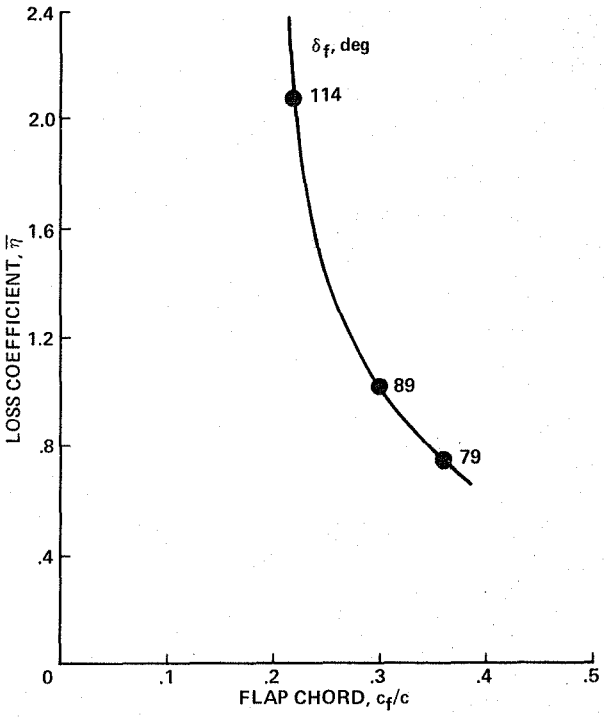

Fig. 24 Effect of flap chord on loss coefficient $\bar{\eta}$ for flow aligned with outflow duct (β = 00): vane-set 6; 1/10-scale channel facility; interpolated and extrapolated results using configurations shown on Fig. 20.

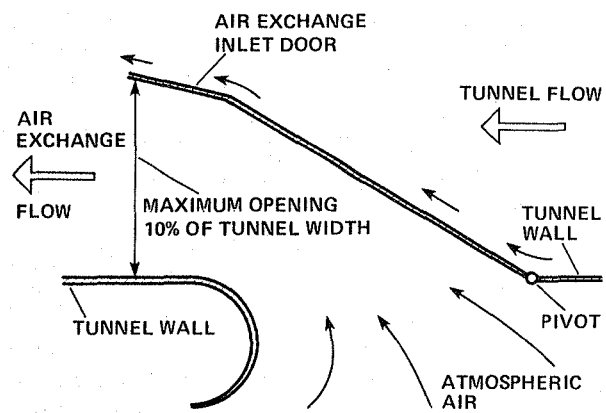

Fig. 25 Air-exchange inlet design (located as shown in Fig. 1).

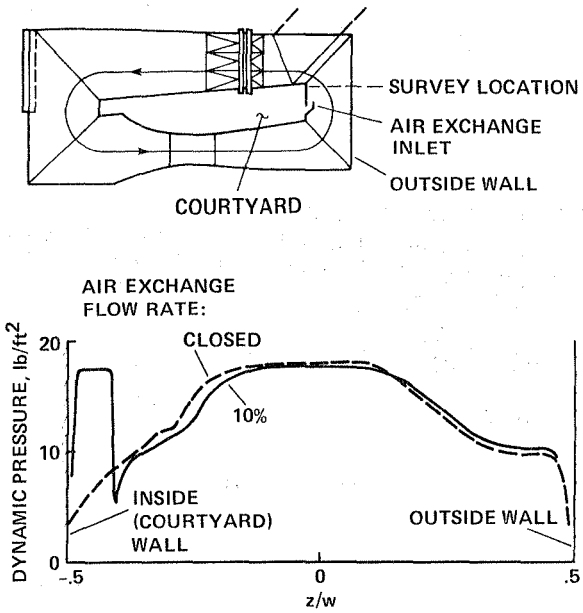

a) Air-exchange inlet location.

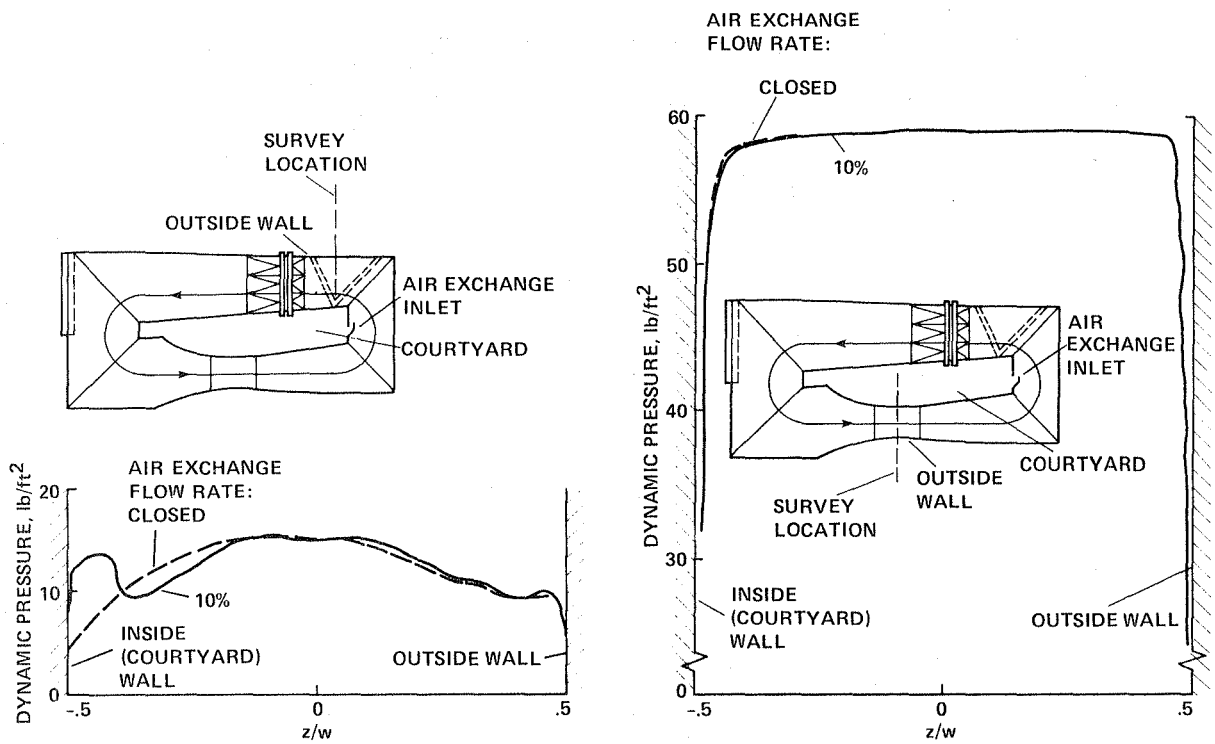

b) Fan-drive inlet location.

c) 40 × 80 test section.

Fig. 26 Effect of air-exchange inlet flow on dynamic pressure profile across wind-tunnel duct: 1/50-scale three-dimensional facility, 40 × 80 mode.

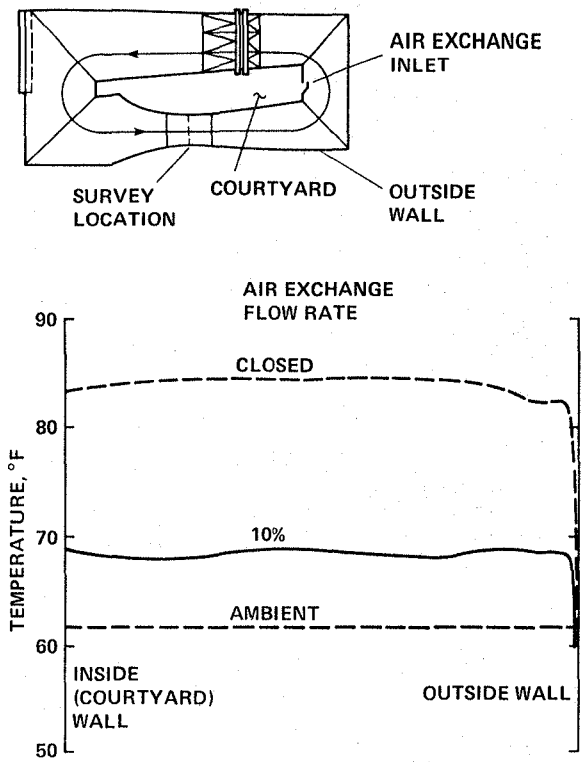

Fig. 27 Effect of air-exchange flow on the temperature distribution in the 40 × 80 test section: 1/50-scale, three-dimensional facility.

1. Report No.	2. Government Accession No.	3. Recipient's Catalog No.
NASA Technical Memorandum 85946		

4. Title and Subtitle	5. Report Date
AERODYNAMIC CHARACTERISTICS OF THE 40- BY 80/80- BY 120-FOOT WIND TUNNEL AT NASA AMES RESEARCH CENTER	April 1984
	6. Performing Organization Code ATP
7. Author(s) Victor R. Corsiglia, Lawrence E. Olson, and Michael D. Falarski	8. Performing Organization Report No. A-9675
	10. Work Unit No. T-3225
9. Performing Organization Name and Address Ames Research Center, Moffett Field, California 94035	11. Contract or Grant No.
	13. Type of Report and Period Covered Technical Memorandum
12. Sponsoring Agency Name and Address National Aeronautics and Space Administration Washington, D.C. 20546	14. Sponsoring Agency Code 505-43-01

15. Supplementary Notes

Point of contact: Victor R. Corsiglia, Ames Research Center, MS 247-1, Moffett Field, CA (415) 965-6677 or FTS 448-6677

16. Abstract

A design and testing program has been undertaken to improve the aerodynamic performance of the 40- by 80/80- by 120-Foot Wind Tunnel at NASA Ames Research Center. Experimental and theoretical results pertaining to both turning-vane performance and air-exchanger performance are presented. Extensive studies have been conducted to develop turning-vane airfoils with improved aerodynamic performance and to insure that this performance is not compromised by interactions between the cascades of airfoils and the duct or diffuser walls within which these cascades are required to operate. Much of the theoretical analysis and design was done by personnel at NASA Lewis Research Center. Because of the nature of the 40- by 80/80-120-Foot Wind Tunnel complex, it was necessary to consider a wide range of vane-set designs. A design has been developed that provides efficient control of the flow at the intersection of the 40 x 80 wind-tunnel circuit and the 80 x 120 wind tunnel-circuit. The airfoil shape and solidity of this design results in a vane set that can accept onset flow at angles ranging from -5° to 55° while maintaining relatively low drag and having only minor variations in the direction of the flow exiting the cascade. A second vane set has been tested for use in a 90° bend. This cascade provides efficient aerodynamic performance yet the airfoil shape can be built using simple fabrication techniques. In a third study, it was shown that the outflow angle from a vane set is an important parameter in determing the tunnel performance downstream of the vane set. Over-turning or under-turning of the flow (measured relatime to the axis of the duct or diffuser downstream from the cascade) results in cross-stream total-pressure gradients that will persist as the flow continues around the circuit of the wind tunnel. Guidelines for minimizing this potential problem are presented. An air-exchange inlet has also been designed and tested that is capable of enchancing flow quality within the wind-tunnel circuit. This air exchanger utilizes the static pressure difference between the wind-tunnel duct and the atmosphere to create a thick wall jet. One important benefit of this wall jet is improved uniformity of the flow entering the fan drive.

17. Key Words (Suggested by Author(s))	18. Distribution Statement
Wind-tunnel design Wind-tunnel aerodynamics	Unlimited Subject Category: 05

19. Security Classif. (of this report)	20. Security Classif. (of this page)	21. No. of Pages	22. Price*
Unclassified	Unclassified	25	A02

*For sale by the National Technical Information Service, Springfield, Virginia 22161

End of Document